Springer

Journal of
Mechanical
Science and
Technology

Journal of Mechanical Science and Technology 22 (2008) 1181~1191

www.springerlink.com/content/1738-494x

LBM simulation on mixing enhancement by the effect of heterogeneous zeta-potential in a microchannel

Jinfen Kang[1], Hyeung Seok Heo[2] and Yong Kweon Suh[1,*]

[1]*Department of Mechanical Engineering, Dong-A University, 840, Hadan-dong, Saha-gu, Busan, 604-714, Korea*
[2]*Tongmyung Mottrol Co., Ltd, 465-3, Naedong, Changwon, Kyungnam, 641-050, Korea*

(Manuscript Received July 9, 2007; Revised February 21, 2008; Accepted March 3, 2008)

Abstract

In this study, we use the lattice Boltzmann method to perform 2D and 3D numerical simulations to investigate the electrokinetic effect on the fluid flow and mixing in a rectangular microchannel. Zeta-potential serves as the main factor representing the electrokinetic effect. The numerical simulations in particular aim at evaluation of the mixing performance of two new designs of electrode distribution in the microchannel. One uses the periodically distributed rectangular electrodes on lateral walls of the microchannel, for which 2D and 3D simulations were implemented with time-periodic application of the electric potential on the electrodes. In another model, a periodic array of trapezoidal electrodes with a constant electric potential on them was attached on the bottom walls, for which 3D simulation was carried out. Through the parametric studies for both designs, it was shown that there exists an optimum parameter value leading to the best mixing performance.

Keywords: Lattice-boltzmann method; Microchannel; Microfluidic mixing; Heterogeneous zeta-potential

1. Introduction

The explosive growth of interest in and the subsequent experimental and/or numerical studies on microfluidics have shed light on the evolution of many disciplines, such as the life sciences, biomedicine and analytical chemistry. For instance, in the processes of research on drug delivery, drug discovery, sample preparation and analysis, cell separation and detection and so on, applications of microfluidics increase the accuracy and efficiency of analysis. Within the whole microfluidic system like lab-on-a-chip, as a critical process of preparation of the reagent, samples usually need to be mixed as fast as possible, prior to further processing. However, due to the small dimensions of the mixers, the flow in a microfluidic system is always laminar. In this case, the fast micromixing must rely, first, on the stretching/folding of fluid blobs usually through the chaotic advection, and secondly on the molecular diffusion across the lengthened interfaces. In this context, the most important issue for the enhancement of the micromixing is how to elaborate fluid flows that lead to chaotic advection; in fact, the total time needed for complete mixing is dominated by the time consumed in stretching the interfaces, and so the vital importance is how to make the interfaces elongated as quickly as possible.

Various mechanisms have been used to improve micromixing. Pressure or electrokinetically driven lamination and repeated splitting/rejoining of the inlet streams help to increase the contact surface between two fluids [1-5]. Fabricating specific geometry like grooves or ribs [6, 7], micromachined stirrer [8] or obstacles [9] in the microchannel can stimulate chaotic advection. Even a droplet of liquid has been used as a mixer by itself [10]. References [11, 12] demonstrate that mixing enhancement can be realized by using unsteady pressure perturbations to generate pulsating flows. Temperature disturbance or the

*Corresponding author. Tel.: +82 51 200 7648, Fax.: +82 51 200 7656
E-mail address: yksuh@dau.ac.kr
DOI 10.1007/s12206-008-0301-4

variation of diffusion coefficient has been known to give an edge to micromixing [13]. The electrohydrodynamical method, first proposed by Tsouris et al. [14] and Moctar et al. [15], is based on the fact that when two fluids having different electrical properties (e.g., conductivity and permittivity) are subjected to an electric field, it exerts different electric forces on the two fluids to make the interfaces stretched and folded to realize fluidic mixing. Dielectrophoretics was also employed in mixing of particles [16, 17]. Magnetohydrodynamics [18-20], acoustics [21, 22] and centrifugal forces [23] are also applicable under specific conditions. Among others, the electrokinetic method, due to its several advantages, is one of the more popular mechanisms employed in micromixing. The advantages include ease of integrating electronic control modules to microfluidic systems and feasibility of providing power to drive fluid flow, and simultaneously, to create mixing with just simple geometries. In this work, we also employed this facile tool to generate efficient micromixing.

In the literature, numerous research reports on employing electoosmotic flow as a tool for mixing are available for reference. Jacobson et al. [24] studied parallel and serial lamination mixers driven by a single voltage source control. Stroock et al. [25] first exposed the effect, on mixing, of the patterned surface charge used to induce heterogeneous surface zeta-potential in a three-dimensional channel. The spatially periodic strips of surface charge subjected to an external electric field applied along the longitudinal direction of the channel were shown to give rise to multidirectional or circulating cellular electro-osmotic flows. Oddy et al. [26] contrived a batch mixer of cavity shape and demonstrated that the flow instability, occurring when an AC voltage is actuated through the cavity, is responsible for the efficient mixing. Qian and Bau [27, 28] designed chaotic electro-osmotic mixers and applied a numerical method to analyze the model. They derived analytical solutions for the simplified two-dimensional cavity models with the aid of Fourier series and superposition principle. In their model, heterogeneous zeta-potentials are applied on the top and bottom walls so that the induced steady as well as unsteady flows give rise to chaotic mixing. Erickson and Li [29] numerically investigated enhancement of mixing in a three-dimensional T-shape microchannel by introducing heterogeneous surface zeta-potential. They studied the mixing behavior by implementing 3D finite-element simulations. Chang and Yang [30] presented a 2D numerical simulation of steady electro-osmotic flows in microchannels with rectangular blocks attached to the upper and lower walls. Heterogeneous surface zeta-potential is induced on the top surface of the rectangular blocks as well as the channel wall. However, the geometry is complex, and a chaotic mixing pattern such as stretching and folding did not take place. Wu and Liu [31] proposed a T-shaped microchannel mixer. On the bottom wall of the channel, they embedded an electrode array composed of a series of asymmetric-herringbone electrodes. The induced zeta-potential's temporal modulation was realized by applying AC voltage, while the spatial modulation was facilitated by the asymmetric-herringbone-electrode structure. Using numerical simulation as well as experiment, they demonstrated that great mixing efficiency could be achieved from their mixers. Pacheco et al. [32] proposed a design in which the surface zeta-potentials on the top and the bottom walls are maintained at constant values. In addition to the steady electric field along the longitudinal direction, which drives the primary flow, a secondary time-dependent external electric field was applied transverse to the flow by alternatively switching on and off the applied DC voltages on electrodes attached to the side walls.

Illuminated by the previous researchers' efforts, we in this study sought more elaborate designs in the distribution of surface charges to enhance micromixing. Specifically, we propose two kinds of rectangular microchannel with heterogeneous zeta-potentials on the channel walls subjected to a uniform longitudinal external electric field. In the first micromixer design, rectangular electrodes are periodically embedded on the surface of the lateral walls. We use AC voltage to control the electrodes, thus leading to temporally periodic change of the surface zeta-potential on the electrodes. Due to not only the uniform electric filed but also the spatial and temporal periodic altering of the zeta-potentials on the channel side walls, there occurs secondary, oscillatory flow in addition to the primary, steady flow. As the second design, trapezoidal electrodes are embedded on the bottom wall of the channel. We apply DC voltage on the electrodes, so that the surface charge value remains constant. As a result of such an arrangement, a spatially periodic distribution of heterogeneous zeta-potential plus a uniform external electric field actuates steady asymmetric cross-flows inside the microchannel. These

multidirectional flows are expected to be greatly beneficial to the micromixing.

Regarding the numerical tool for the analysis, we applied LBM, which has been demonstrated in many research works to be simple, accurate and efficient for analysis of a variety of fluidic applications. There are several good references discussing the application of LBM to electro-osmotic flows in microfluidic channels [33, 34] and micromixing in electro-osmotic flows [35, 36]. In Tian et al.'s paper, two-dimensional electro-osmotic flow in microchannels with non-uniform surface zeta-potentials was investigated by LBM. They solved the Poisson-Boltzmann equation for electric potential and ion distribution, while the mixing process was assessed only by streamlines.

In order to reduce the cost and difficulty of analysis, we applied the steady electro-osmotic slip velocity calculated from the Helmholtz-Smoluchowski equation [37] assuming that the zeta-potential is directly related to the applied slip velocity value. In this way, not only can we conveniently apply LBM to analysis of the fluid flow and its mixing process but also pay more attention to the mixing behavior inside the three dimensional microchannel mixers and to the enhancement of mixing efficiency. The enhancement of mixing in our model is affected by several factors including geometry of the electrodes themselves as well as the spacing between electrodes and the magnitude and temporal modulation of the zeta-potential on the electrodes, etc. So, we carried out a parameter study in order to pursue an optimum parameter set leading to the best mixing performance.

The rest of this paper is organized as follows. Section 2 describes the geometry of two new kinds of rectangular microchannel mixer. Section 3 presents the framework of the lattice Boltzmann method applied and the quantitative evaluation method for the mixing performance. We provide the simulation results and discussions in section 4 and give conclusions in the last section.

2. Microchannel flow models

2.1 2D and 3D time-periodic flows

The first design proposal as a model for a mixer is composed of a rectangular microchannel with rectangular electrodes embedded on the side walls as shown in Fig. 1. When a steady electric field E is applied in the electrolyte within the channel along the longitudinal (X-) direction, due to the electrokinetic forces acting on the clustered (usually positive) ions in the EDL (electric double layer) very near the channel walls, the whole fluid moves downstream with uniform velocity profile across the channel, which is called 'electro-osmosis'. The velocity determined at the interface between the EDL and the bulk region is called slip velocity [38]. Since the thickness of EDL is usually very small ($10\text{Å}-100\text{Å}$) compared with the channel space, we do not take into account the detailed flow behavior within EDL, and we use the slip velocity as the boundary condition on the wall in describing the bulk fluid flows. On the other hand, alternating current with a relatively low frequency is applied to the electrodes, so that the zeta-potential on the electrodes is modulated in time. As shown in Fig. 1, such an arrangement gives rise to a steady flow driven by the slip velocity U_0^* on the normal wall surface plus the oscillatory flow driven by the time-

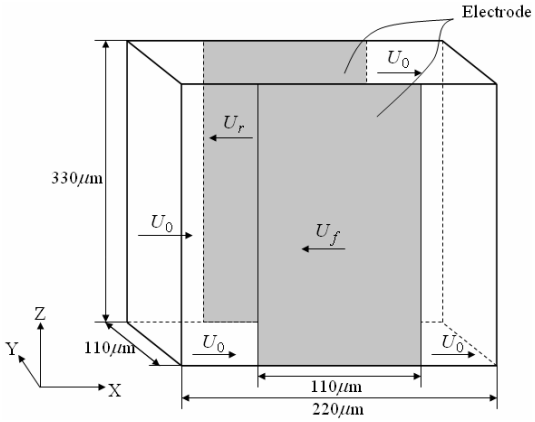

Fig. 1. Perspective view of microchannel with periodically distributed rectangular electrodes representing the first channel design in this study.

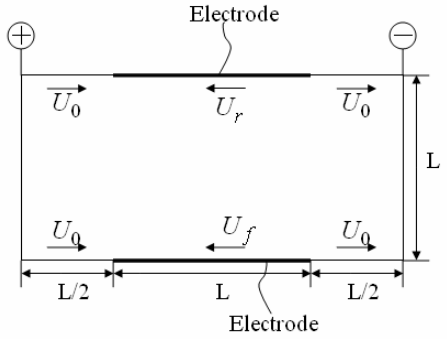

Fig. 2. Simplified 2D microchannel model of Fig. 1.

periodic application of the electric potential on the electrodes. If the channel height is large enough, then 2D calculation is relevant; the simplified 2D model is demonstrated in Fig. 2.

With an electric field E and zeta-potential ζ, the electro-osmotic velocity U^*, also known as the slip velocity, can be calculated by using the Helmholtz-Smoluchowski Eq. [38]:

$$U^* = -\frac{\varepsilon_r \varepsilon_0}{\mu} E\zeta \tag{1}$$

Here, ε_r is the dielectric constant of the fluid, ε_0 the permittivity of vacuum, μ the dynamic viscosity of the fluid. Whereas the zeta-potential on the normal walls is maintained at a constant value say $\zeta = \zeta_N$, those on the electrodes are modulated in time by application of alternating voltages. This will make the slip velocity also change periodically. The slip velocity on the normal wall, i.e., U_0^*, is calculated by applying $\zeta = \zeta_N$ to Eq. (1).

Prior to the LBM simulation, we convert U_0^* in the physical unit into U_0 in the lattice unit by using a reference velocity c^*, which is called speed of sound and calculated by $\delta x^* / \delta t^*$, where δx^* is the size of the lattice and δt^* is the time step for one complete cycle of calculation; $U_0 = U_0^* / c^*$. The velocities on the electrode walls of the microchannel can be given in the lattice unit as follows.

$$U_f = \left[1 - \gamma_f \cos^2(\pi t / T)\right] U_0$$
on the front electrodes, (2a)

$$U_r = \left[1 - \gamma_r \sin^2(\pi t / T)\right] U_0$$
on the rear electrodes, (2b)

where T is the time period of zeta-potential modulation on the electrodes and γ_f and γ_r the relative magnitude of zeta-potential on the front and rear electrodes adjustable by the applied voltages, respectively, referring to that of the normal wall. We define, for a positive constant n, $T = nT_0$, where $T_0 = D_h / U_0$ is the characteristic time scale and D_h the hydraulic diameter of the channel's cross section; all are in the lattice unit. As per the main purpose of this study, we aim to find an optimum value of n that yields the best mixing performance. In proposing the modulation of the slip velocity by Eqs. (2a) and (2b), we assume that the zeta potential on the electrode surface can be controlled without difficulty by adjusting the applied voltage in time; of course, controlling such zeta potential may require a sophisticated structure in practice.

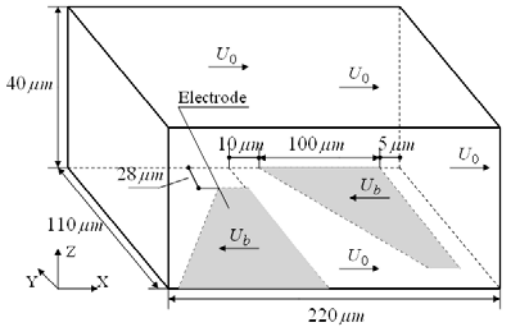

Fig. 3. Perspective view of the microchannel with periodically distributed trapezoidal electrodes on the bottom wall.

2.2 3D steady flows

In the second channel design, the microchannel has a periodic array of trapezoidal electrodes on the bottom wall (Fig. 3). Such an arrangement turns out to generate a cross flow. The slip velocity on the normal wall is the same as in Eq. (1) and the velocity on the electrode walls is given as follows.

$$U_b = \gamma_b U_0 \qquad \text{on the bottom electrodes,} \tag{3}$$

As implied in the boundary condition Eq. (3), the electric potential is applied on the electrodes with DC. The constant γ_b represents the relative magnitude of the potential on the electrodes.

3. Numerical method

In the LBM approach, one solves the kinetic equation for the particle velocity distribution function f. The macroscopic quantities (such as mass density ρ and momentum density $\rho\mathbf{u}$) can then be obtained by evaluating the hydrodynamic moments of the distribution function. There are several models for LBM currently in use to simulate fluid problems. In the present simulation, we applied the most popular, Bhatnagher-Gross-Krook (BGK) collision operator [39], and adopted the modified equilibrium distribution function, which was proposed by He and Luo [40] for incompressible flow. The distribution function is determined by the following evolution equation.

$$f_\alpha(\mathbf{x} + \mathbf{e}_\alpha \delta t, t + \delta t) - f_\alpha(\mathbf{x}, t) = -\frac{1}{\tau}\left[f_\alpha(\mathbf{x}, t) - f_\alpha^{eq}(\mathbf{x}, t)\right] \tag{4}$$

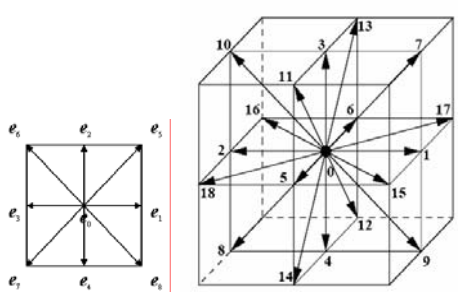

Fig. 4. Discrete velocity vectors for D2Q9 (left hand side) and D3Q19 (right hand side) lattice.

In the above evolution equations, $\tau = 3\nu + 0.5$ is the dimensionless relaxation time, ν the kinetic viscosity, $\mathbf{x}$ the grid point coordinate, δt the time step, f_α the distribution function, and f_α^{eq} the equilibrium distribution function in the $\alpha-$th direction to be given by

$$f_\alpha^{eq} = \omega_\alpha \left\{ \rho + \rho_0 \left[\frac{1}{c_s^2}\mathbf{e}_\alpha \cdot \mathbf{u} + \frac{1}{2c_s^4}(\mathbf{e}_\alpha \cdot \mathbf{u})^2 - \frac{1}{2c_s^2}(\mathbf{u}\cdot\mathbf{u}) \right] \right\} \tag{5}$$

where $\mathbf{u}$ is the macroscopic velocity, ρ the density of fluid, ω_α the weighting coefficient, and $\mathbf{e}_\alpha$ denotes the discrete velocity vectors, which are shown in Fig. 4 for two-dimensional nine-velocity lattice model (D2Q9) and three-dimensional nineteen-velocity lattice model (D3Q19). c_S is the sound speed depending on the specific choice of discrete velocity $\mathbf{e}_\alpha$, here, $c_S = 1/\sqrt{3}$.

The weighting coefficients for D2Q9 are: $\omega_\alpha = 4/9$ for $\alpha = 0$, $\omega_\alpha = 1/9$ for $\alpha = 1,2,3,4$, and $\omega_\alpha = 1/36$ for $\alpha = 5,6,7,8$. For D3Q19, they are: $\omega_\alpha = 1/3$ for $\alpha = 0$, $\omega_\alpha = 1/18$ for $\alpha = 1,2,\cdots,6$, and $\omega_\alpha = 1/36$ for $\alpha = 7,8,\cdots,18$.

The fluid density and momentum are evaluated by the following formulas:

$$\rho = \sum_\alpha f_\alpha \tag{6}$$

$$\rho \mathbf{u} = \sum_\alpha \mathbf{e}_\alpha f_\alpha \tag{7}$$

To evaluate the mixing performance, we numerically simulated the concentration transport of species. In general, species are transported by convection and diffusion. We assume that the species transport is passive. The proposed evolution equation for the transport of the species i has the following form [36, 41].

$$g_\alpha^i(\mathbf{X}+\mathbf{e}_\alpha\delta t, t+\delta t) - g_\alpha^i(\mathbf{X},t) = -\frac{1}{\tau_i}\left[g_\alpha^i(\mathbf{X},t) - g_\alpha^{i,eq}(\mathbf{X},t) \right] \tag{8}$$

where $\tau_i = 3D_i + 0.5$ is the dimensionless relaxation time for the calculation of concentration, D_i the diffusivity, g_α^i the distribution function of the concentration along the $\alpha-$th direction, and $g_\alpha^{i,eq}$ the equilibrium distribution function given as

$$g_\alpha^{i,eq} = \omega_\alpha c_i \left[1 + \frac{1}{c_s^2}\mathbf{e}_\alpha \cdot \mathbf{u} + \frac{1}{2c_s^4}(\mathbf{e}_\alpha \cdot \mathbf{u})^2 - \frac{1}{2c_s^2}(\mathbf{u}\cdot\mathbf{u}) \right] \tag{9}$$

Similar to Eq. (6), c_i, the concentration of species i, is calculated by using:

$$c_i = \sum_\alpha g_\alpha^i \tag{10}$$

In order to evaluate the quantitative effect of mixing, the mixing index, which has already been used by previous researchers [42, 43], is employed:

$$D = \sqrt{\frac{1}{N}\sum_{i,j}^{N}\left(1 - c(i,j)/\bar{c}\right)^2} \tag{11}$$

where, $c(i,j)$ is the concentration on the node (i,j), $\bar{c}$ the spatial average of concentration for the whole fluid domain, and N the total number of grid points, i.e. $N = I \times J$. A lower mixing index indicates a better mixing effect.

4. Numerical results and discussions

4.1 2D and 3D time-periodic flows

First, we present the 2D numerical results obtained for the microchannel depicted in Fig. 2. The number of grids is fixed at 200×100, the Reynolds number $\mathrm{Re} = U_0 L/\nu$ at 0.8, and the slip velocity on the wall at $U_0 = 0.005$. Since the length scale for 2D case is $L = 100$, we get the viscosity $\nu = 0.625$. Then, τ the relaxation time in the equation for the particle distribution function f becomes 2.375. The Peclet number, $\mathrm{Pe} = U_0 L/D_i$, is fixed at $\mathrm{Pe} = 1\times10^4$, from which we can compute the diffusivity D_i. This in turn gives $\tau_i = 3D_i + 0.5 = 0.50015$. The magnitude of τ_i influences the stability of the LBM simulation,

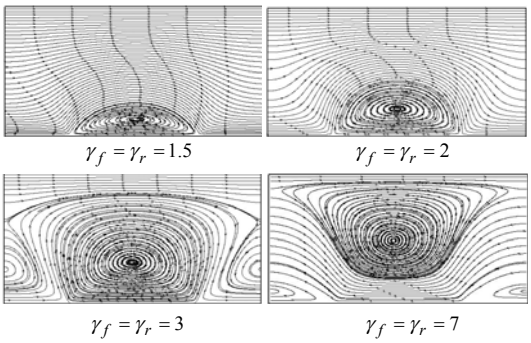

Fig. 5. Instantaneous streamlines of the 2D time-periodic flow at $t = 0$ with four different values of γ_f and γ_r.

implying that there is a high limit of Pe we can use. But, fortunately in 2D case, the stability is not so sensitive to Pe. As the boundary condition for f and g, we employed extrapolation schemes [44]. For f, we applied the velocity $U_0 = 0.005$ to the normal walls and U_f and U_r given by (2a) and (2b) to the electrodes. Zero flux condition was applied for g. A periodic boundary condition was used at upstream and downstream ends of the channel.

Fig. 5 shows the streamlines of the basic flows at various values of γ_f and γ_r. The basic flow is composed of the primary, uniform flow and the back flow driven locally by the electrodes. As a result, the region adjacent to the electrodes is occupied by a recirculating cell. As the zeta-potential is increased, the size of the cell also increases. It turns out that in general the mixing is enhanced when the magnitudes of γ_f and γ_r are larger. However, such a setup leads to a lower flow rate, and so we must compromise between the mixing effect and the flow rate.

We will show in the following the numerical results of the parametric study. In the first part of this study, we fixed $\gamma_f = \gamma_r = 2$ and investigated the mixing performance under the influence of other factors.

Evolution of the concentration patterns is shown typically at $T = 3T_0$ in Fig. 6; the figure shows the patterns after some multiple of periods. The grey scale in the figures indicates the magnitude of the concentration $c(i, j)$. The initial concentration is set as $c_0(i, j) = 1$ for the front half of the domain (in the figure 'bottom' half) and $c_0(i, j) = 0$ for the rear half ('top' half); here "front" and "rear" are used to be consistent with the 3D case. Apparently, there occurs chaotic mixing demonstrated by the stretching and folding of passive materials. Also, we can see that the patterns tend to a steady structure called 'invariant

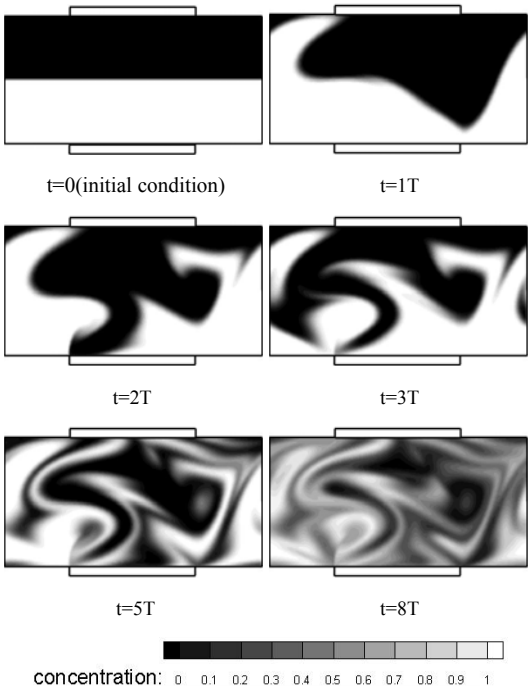

Fig. 6. Time evolution of the concentration distribution for 2D time-periodic flow ($\mathrm{Re} = 0.8$, $\mathrm{Pe} = 10{,}000$, $\mathrm{T} = 3\mathrm{T}_0$, $\gamma_f = \gamma_r = 2$).

manifold'. It also shows a gradual approach to a uniform concentration with $c_0 = 1/2$ implying good mixing.

As is common for most time-periodic flows, the modulation period T is expected to be the most important parameter regarding optimization for the best mixing. So, simulation is performed to investigate the effect of T on the mixing index. Here again the relative magnitude of the zeta-potentials on the electrodes is fixed at $\gamma_f = \gamma_r = 2$. In Fig. 7, we show time evolutions of mixing indices for various values of T. Mixing performance appears to be sensitive to T, and more importantly its effect is not monotonic implying that there exists an optimum value of T that leads to the best effect. In this graph, we see that the mixing index is the lowest with $T = 3T_0$ at the final time $t = 50T_0$. The values of mixing index D at $t = 50T_0$ for various T values are plotted in Fig. 8. We obviously find that the mixing index is smallest at $T = 3T_0$

We also simulated this 2D problem using a finite volume method (FVM) with standard schemes such as centered difference for the spatial discreti-

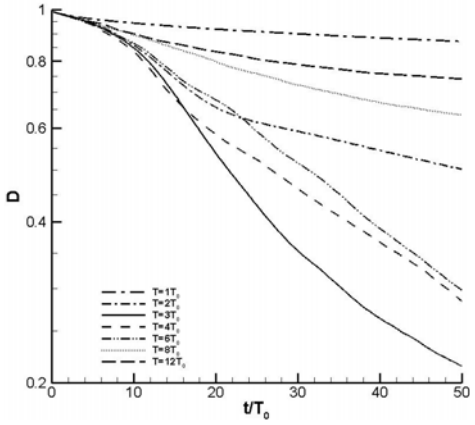

Fig. 7. Evolution of mixing indices for different T for 2D time-periodic flow ($\mathrm{Re}=0.8$, $\mathrm{Pe}=10{,}000$, $r_f = r_r = 2$).

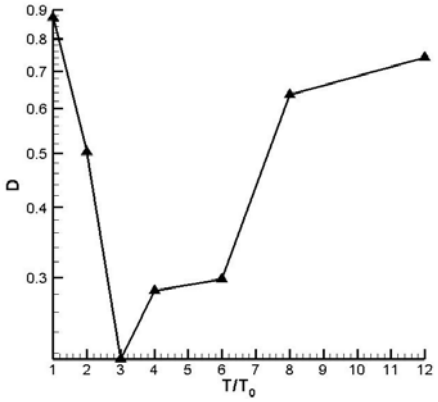

Fig. 8. Variation of mixing indices at $t = 50T_0$ for different T for 2D time-periodic flow ($\mathrm{Re}=0.8$, $\mathrm{Pe}=10{,}000$, $\gamma_f = \gamma_r = 2$).

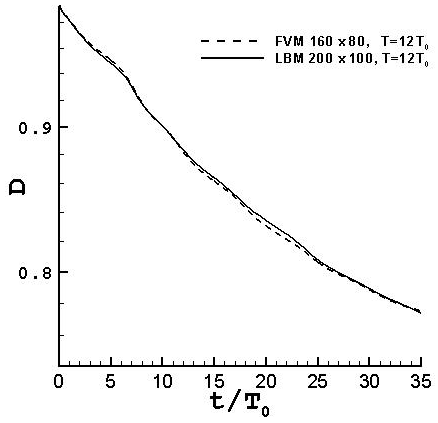

Fig. 9. Comparison of mixing indices obtained by FVM and LBM for $T = 12T_0$ with different grid numbers for 2D time-periodic flow.

zation and incomplete Cholesky conjugate gradient method for the pressure, etc. We compared the mixing index obtained by LBM with that by FVM. Fig. 9 shows the comparison for a typical parameter set $T = 12T_0$ and $\mathrm{Pe}=10{,}000$. Overall, the two results are in a good agreement, so we can judge that our LBM code is reliable.

For 3D time-periodic flows, we carried out a simulation under the following conditions. The number of grids is set at $56\times28\times84$, the Reynolds number at $\mathrm{Re}=2$, the slip velocity on the wall at $U_0 = 0.02$, viscosity at $\nu = 0.42$, and hydraulic diameter at $D_h = 42$. Then these give the relaxation time of the evolution of the particle distribution function f as $\tau = 1.76$. As the boundary condition for f , we applied the extrapolation scheme as done with the 2D simulation, and for g we applied the no-flux condition following the simplest method as described by Succi [45]. It turned out that the 3D LBM algorithm was more sensitive to the Peclet number with respect to the numerical stability than 2D; so, we set $\mathrm{Pe}=4750$ as the upper limit of the stable calculation.

We display in Fig. 10 the calculated concentration patterns on the central plane $Z = H/2$ at $T = 3T_0$,

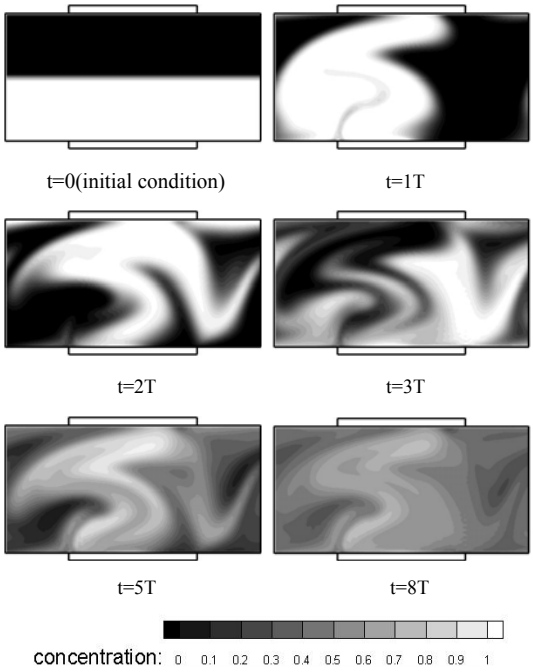

Fig. 10. Time evolution of the concentration patterns on the XY plane at $Z = H/2$ for 3D time-periodic flow. ($T = 3T_0$, $\mathrm{Re}=2$, $\mathrm{Pe}=4750$, $\gamma_f = \gamma_r = 2$)

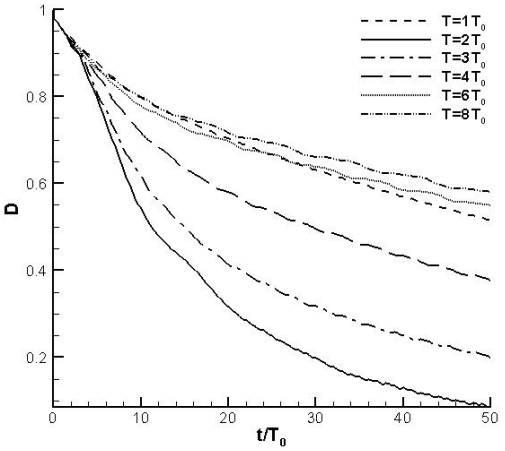

Fig. 11. Mixing indices with different T for 3D time-periodic flow ($\mathrm{Re}=2$, $\mathrm{Pe}=4750$, $\gamma_f=\gamma_r=2$).

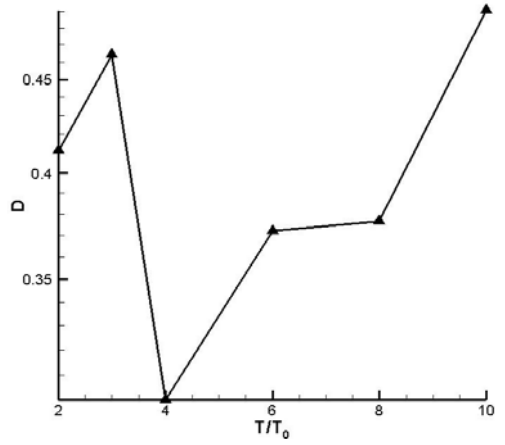

Fig. 12. Variation of mixing indices for different T for 3D time-periodic flow at t=32 T_0 ($\mathrm{Re}=2$, $\mathrm{Pe}=4750$, $\gamma_f=\gamma_r=2$).

where H denotes the total height of the channel. Except for the initial development, the asymptotic striation patterns look similar to the ones obtained for 2D case, i.e., Fig. 6. This is plausible because the channel is set high enough that the end-wall effect becomes less significant. On the other hand, the 3D case shows more rapid dispersion than 2D. This is also relevant because Pe is set much smaller than 2D. On the other hand, rather coarser grids used in 3D calculation may be another factor causing such rapid dispersion.

Fig. 11 shows the time evolution of mixing indices for various Td values. This figure reveals a faster increase of D than the 2D case, i.e., Fig. 7, especially in the early time of the concentration dispersion. This indicates that the dispersion in the early time is governed by diffusion rather than advection. We also see that, like the previous 2D case, there may exist an optimum T value for the best mixing performance. Fig. 12 indicates that the optimum value is $T=4T_0$. This value is a little bit different from the result of the 2D simulation, $T=3T_0$. Moreover, dependence of D on the T value for the 3D case is not as significant as the 2D case. The discrepancy between the 2D and 3D results is obviously due to the difference in the Peclet number and the end-wall effects. Nevertheless, because applying the 2D model can simplify the numerical calculation and reduce the time cost by almost 10 times, employing such a periodical and symmetrical model using 2D simplification is beneficial.

4.2 3D steady flows

We now present the simulation results of the fluid flow and mixing process of the 3D steady flow model. As the steady slip velocity on the trapezoidal electrodes, we applied the magnitude calculated from (3). In the parameter study, the effect of γ_b on the mixing is investigated. The fluid space is discretized by a $154\times77\times28$ grid system. We set Reynolds number at $\mathrm{Re}=2$, the slip velocity at $U_0=0.025$, the viscosity at $\nu=0.513$ and the hydraulic diameter at $D_h=41.07$. The relaxation time of the particle distribution function f is computed as $\tau=2.04$. When we used the bounce-back scheme as the boundary condition for g, we experienced some wiggles near the boundaries. Further, applying an extrapolation scheme to f and g simultaneously gives rise to stability problem at high Peclet numbers. Therefore, there is a bottleneck of Pe. In the present calculation, we fixed Pe=237. The concentration distribution patterns on the XY section at the height of $Z=H/3$ are demonstrated in Fig. 13.

The patterns on the left hand side column correspond to the LBM results, whereas the right hand side to the numerical results calculated by the commercial code CFX under the same conditions. Comparison of the two results shows good agreement. From Fig. 14 and 15 showing the mixing indices with different magnitude γ_b, we can see that the mixing is best when the magnitude of slip velocity on the electrodes is given $\gamma_b=-3$. Fig. 16 shows the effect of γ_b on the flow rate. At $\gamma_b=-3$, in which the best mixing is attained, the flow rate is reduced to $1/3$ of that with

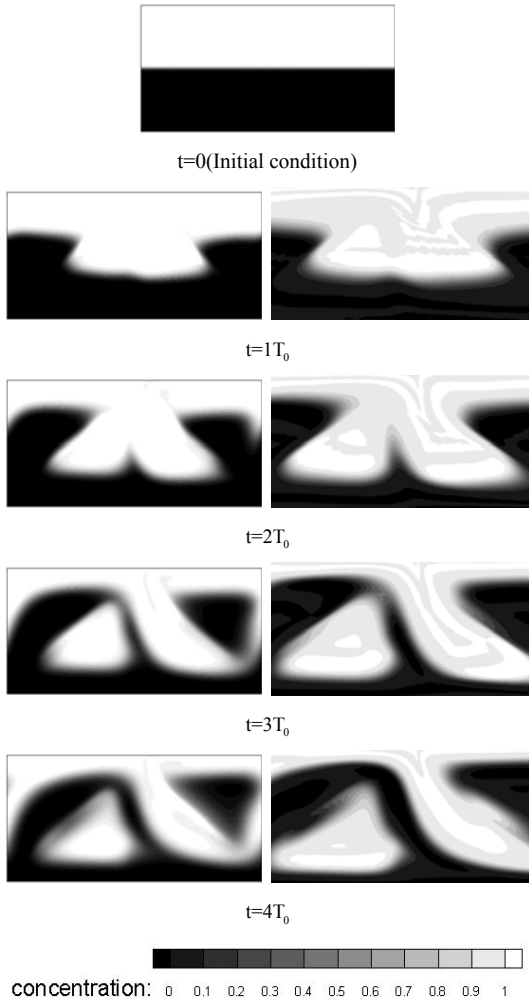

Fig. 13. Time evolution of the concentration distribution on the plane $Z = H/3$ for 3D steady flow at $\gamma_b = -2$: L-H-S patterns are obtained by LBM; R-H-S patterns are calculated by CFX ($\mathrm{Re} = 2$, $\mathrm{Pe} = 237$).

the case of simple channel flow ($\gamma_b = 1$). Here again, the channel designer must compromise between the mixing effect and the fluid transport.

5. Conclusions

We gave out two new designs of a microchannel mixer with delicate distributed electrodes on the channel wall to generate heterogeneous zeta-potential, which is demonstrated to give rise to an effective enhancement of micro fluidic mixing. We applied LBM to simulate both fluid flow and its mixing process and carried out a parameter study to investigate the relationship between mixing performance and the impact factors including relative magnitude and modulation period of the zeta-potential on the electrodes. The concentration patterns at different timesteps and the mixing indices lead us to clear recognition of the chaotic mixing behavior and mixing quality. We found optimized values for the best mixing performance through the parameter studies.

Acknowledgments

This work was supported by the Korea Science and Engineering Foundation(KOSEF) through the National Research Laboratory Program funded by the Ministry of Science and Technology (No. 2005-1091).

References

[1] F. G. Bessoth, A. J. DeMello and A. Manz, Microstructure for efficient continuous flow mixing, *Anal. Commun.,* 36 (1999) 213-215.

[2] B. L. Gray, D. Jaeggi, N. J. Mourlas, B. P. van Drieenhuizen, K. R. Williams, N. I. Maluf and G. T. A. Kovacs, Novel interconnection technologies for integrated microfluidic systems, *Sensors and Actuators*(A), 77 (1999) 57-65.

[3] V. Mengeaud, J. Josserand and H. H. Girault, Mixing processes in a zigzag microchannel: Finite element simulation and optical study, *Anal. Chem.,* 74 (2002) 4279-4286.

[4] M. S. Munson and P. Yager, Simple quantitative optical method for monitoring the extent of mixing applied to a novel microfluidic mixer, *Anal. Chim. Acta.,* 507 (2004) 63-71.

[5] D. S. Kim, S. H. Lee, T. H. Kwon and C. H. Ahn, A serpentine laminating micromixer combining splitting/recombination and advection, *Lab Chip,* 5 (2005) 739-747.

[6] A. D. Stroock, S. K. W. Dertinger, A. Ajdari, I. Mezic, H. A. Stone and G. M. Whitesides, Chaotic mixer for microchannels, *Science,* 295 (2002) 647-651.

[7] L. H. Lu, K. S. Ryu and C. Liu, A magnetic microstirrer and array for microfluidic mixing, *J. MEMS,* 11(5) (2002) 462-469.

[8] H. Wang, P. Lovenitti, E. Harvey and S. Masood, Optimizing layout of obstacles for enhanced mixing in microchannels, *Smart Mater. Struct*., 11 (2002) 662-667.

[9] P. B. Howell Jr., D. R. Mott, S. Fertig, C. R. Kaplan,

J. P. Golden, E. S. Oran and F. S. Ligler, A microfluidic mixer grooves placed on the top and bottom of the channel, *Lab Chip,* 5 (2005) 524-530.

[10] H. Song, M. R. Bringer, J. D. Tice and C. J. Gerdts, Experimental test of scaling of mixing by chaotic advection in droplets moving through microfluidic channels, *Appl. Phys. Lett.,* 83 (2003) 4664-4666.

[11] T. Fujii, Y. Sando, K. Higashino and Y. Fujii, A plug and play microfluidic device, *Lab Chip,* 3 (2003) 193-197.

[12] N. Z. Niu and Y. K. Lee, Efficient spatial-temporal chaotic mixing in microchannels, *J. Micromech. Microeng.,* 13 (2003) 454-462.

[13] N. T. Nguyen and Z. Wu, Micromixers-a review, *J. Micromech. Microeng.,* 15 (2005) R1-R16.

[14] C. Tsouris, C. T. Culbertson, D. W. DePaoli, S. C. Jacobson, V. F. de Almeida and J. M. Ramsey, Electrohydrodynamic mixing in microchannels, *AIChE J.,* 49(8) (2003) 2181-2186.

[15] A. O. E. Moctar, N. Aubry and J. Batton, Electrohydrodynamic micro-fluidic mixer, *Lab Chip,* 3 (4) (2003) 273-280.

[16] Y. K. Lee, J. Deval, P. Tabeling and C. M. Ho, Chaotic mixing in electrokinetically and pressure driven micro flows, *The 14th IEEE Workshop on MEMS,* (2001) 483-486.

[17] J. Deval, P. Tabeling and C. M. Ho, A dielectrophoretic chaotic mixer, *Proc. MEMS'02, 15th IEEE Int. Workshop,* (2002) 36-39.

[18] H. Suzuki and C. M. Ho, A magnetic force driven chaotic micro-mixer, *Proc 15th IEEE Int. Conf. on Micro Electro Mechanical Systems(C), Las Vegas,* (2002) 40-43.

[19] H. H. Bau J. Zhong and M. Yi, A minute magneto hydrodynamic (MHD) mixer, *Sensors and Actuators*(B), 79 (2001) 207-215.

[20] S. Qian, J. Zhu and H. H. Bau, A stirrer for magnetohydrodynamically controlled minute fluidic networks, *Phys. Fluids,* 14(10) (2002) 3584-3592.

[21] K. Yasuda, Non-destructive, Non-contact handling method for biomaterials in micro-chamber by ultrasound, *Sensors and* Actuators (B), 64 (2000) 128-135.

[22] G. G. Yaralioglu, I. O. Wygant, T. C. Marentis and B. T. Kburi-Yakub, Ultrasonic mixing in microfluidic channels using integrated transducers, *Anal. Chem.,* 76 (2004) 3694-3698.

[23] M. G. A. Geipel, R. R. Zengerle and J. Ducree, Batch-mode mixing on centrifugal microfluidic platforms, *Lab Chip,* 5 (2005) 560-565.

[24] S. C. Jacobson, T. E. Mcknight and J. M. Ramsey, Microfluidic devices for electrokinetically driven parallel and serial mixing, *Anal. Chem.,* 71 (1999) 4455-4459.

[25] A. D. Stroock, M. Weck, D. T. Chiu, W. T. S. Huck, P. J. A. Kenis, R. F. Ismagilov and G. M. Whitesides, Patterning electro-osmotic flow with patterned surface charge, *Phys. Rev. Lett.,* 84 (15) (2000) 3314-3317.

[26] M. H. Oddy, J. G. Santiago and J. C. Mikkelsen, Electrokinetic instability micromixing, *Anal. Chem*., 73 (2001) 5822-5832.

[27] S. Qian and H. H. Bau, A Chaotic electroosmotic stirrer, *Anal. Chem.,* 74 (2002) 3616-3625.

[28] S. Qian and H. H. Bau, Theoretical investigation of electro-osmotic flows and chaotic stirring in rectangular cavities, *Appl. Math. Modelling*, 29(8) (2005) 726-753.

[29] D. Erickson and D. Li, Influence of surface heterogeneity on electrokinetically driven microfluidic mixing, *Langmuir,* 18 (2002) 1883-1892.

[30] C. C. Chang and R. J. Yang, Computational analysis of electrokinetically driven flow mixing in microchannels with patterned blocks, *J. Micromech. Microeng.,* 14 (2004) 550-558.

[31] H. Y. Wu and C. H. Liu, A novel electrokinetic micromixer, *Sensors and Actuators* (A), 118 (2005) 107-115.

[32] J. R. Pacheco, K. P. Chen and M. A. Hayes, Rapid and efficient mixing in a slip-driven three-dimensional flow in a rectangular channel, *Fluid Dynamics Research,* 38 (2006) 503-521.

[33] D. Hlushkou, D. Kandhai and U. Tallarek, Coupled lattice-Boltzmann and finite-difference simulation of electroosmosis in microfluidic channels, *Int. J. Numer. Meth. Fluids,* 46 (2004) 507-532.

[34] J. K. Wang, M. Wang and Z. Li, Lattice Poisson-Boltzmann simulations of electro-osmotic flows in microchannels, *J. Colloid Interface Sci.,* 296 (2006) 729-736.

[35] F. Tian, B. Li and D. Y. Kwok, Tradeoff between mixing and transport for electroosmotic flow in heterogeneous microchannels with nonuniform surface potentials, *Langmuir,* 21 (2005) 1126-1131.

[36] J. Wang, M. Wang and Z. Li, Lattice Boltzmann simulations of mixing enhancement by the electro-osmotic flow in microchannels, *Modern Physics Letters B,* 19 (2005) 1515-1518.

[37] R. F. Probstein, *Physicochemical Hydrodynamics: An Introduction* (2nd Ed.), New York: Wiley and

Sons, Inc., (1994).

[38] D. Li, *Electrokinetics in Microfluidics,* Elsevier Academic Press, (2004) 110-120.

[39] Y. H. Qian, D. D'Humieres and P. Lallemand, Lattice BGK models for Navier-Stokes equation, *Europhys. Lett.,* 17 (1992) 479-484 .

[40] X. He and L. Luo, Lattice Boltzmann model for the incompressible Navier-Stokes equation, *J. Stat. Phys.,* 88 (1997) 927-944.

[41] A. Cali, S. Succi, A. Cancelliere, R. Benzi and M. Gramignani, Diffusion and hydrodynamic dispersion with the lattice Boltzmann method, *Phys. Rev., A* 45 (1992) 5771-5774.

[42] Y. K. Suh, On the problem of using mixing index based on the concentration dispersion, *Trans. KSME*(B), 30 (2006) 796-805.

[43] Y. Kim, S. J. An and J. Maeng, The effect of Karman vortex for mixing in a micro-channel with an oscillating micro-stirrer, *Trans. KSME*(B), 30 (2) (2006) 144-152.

[44] Z. Guo, C. Zheng and B. Shi, An extrapolation method for boundary condition in lattice Boltzmann method, *Phys. Fluids,* 14 (6) (2002) 2007-2010.

[45] S. Succi, *The Lattice Boltzmann Equation for Fluid Dynamics and Beyond,* Oxford: Clarendon Press, (2001) 84-87.